DOI: 10.1002/anie.201409835

Metallic States

Insulating or Metallic: Coexistence of Different Electronic Phases in Zinc Clusters**

Andrés Aguado, Andrés Vega, Alexandre Lebon, and Bernd von Issendorff*

Abstract: *How many of the several attributes of the bulk metallic state persist in a nanoparticle containing a finite number of atoms of a metallic element? Do all those attributes emerge suddenly at a well-defined cluster size or do they rather evolve at different rates and in a broad size range? These fundamental questions have been addressed through a conjoint experimental/theoretical investigation of zinc clusters. We report the observation of novel coexistence phenomena involving different electronic phases: for some sizes, metallic and insulating electronic states coexist within a single, Janus-like, nanoparticle; for the rest of sizes, we report the coexistence of two weakly interacting metallic phases with different dimensionalities, localized at the shell and the core of the nanoparticle. These fascinating features are due to an anomalously long core–shell separation that equips the shell and core regions with largely independent structural, vibrational, and thermal properties.*

The concept of metallicity becomes elusive at the nanoscale. The standard definition in terms of a finite density of electronic states (EDOS) at the Fermi level and the concomitant electrical conductivity is useful only in the bulk limit where the EDOS is continuous. But nanoparticles will in general display a gap at the Fermi level because their associated EDOS is discrete. It may be argued that a nanoparticle becomes metallic-like when the thermal energy becomes comparable with the size of the gap, but that would imply to accept that the criterion for metallicity is temperature-dependent. Issendorff and Cheshnovsky[1] avoided this problem by defining clusters with a gap smaller than the Kubo gap[2] as metallic in a practical sense ($E_{gap} \leq 4E_F/3N$, with E_F the Fermi energy of the bulk material and N the number of atoms in the nanoparticle). This criterion for example can be used to define a critical size for the metal–insulator transition in divalent (ns^2) metals, where the broadening of the occupied band formed from the atomic s-orbitals and the empty band formed from the atomic p-orbitals leads to a decrease of the gap between the two bands with size. The critical sizes found this way are $N = 400$ for Hg,[3] $N = 32$ for Zn,[4] or $N = 18$ for Mg.[5] A problem with this criterion is that clusters of simple metals like sodium (as well as larger Mg or Zn clusters) exhibit an electron shell structure, which leads to large gaps at the Fermi level for certain closed shell sizes. In principle such cluster sizes would be defined as insulating.

It might therefore be sensible to consider other traditional criteria for metallicity as well, as they might be met even by such types of insulating clusters: 1) electronic screening; it is almost perfectly metallic for example in sodium nanoparticles, even the smallest ones;[6–9] 2) shell structure; the electron shell structure in the cluster EDOS indicates the interaction of delocalized electrons with the cluster boundary, and can be used to determine parameters like the electron effective mass or the interaction strength with the ionic cluster structure, which gives hints at the degree of metallicity (a free-electron-like shell structure, though, is only a sufficient, but not necessary condition; open d-shell transition-metal clusters, for example, exhibit a large density of states at the Fermi level, but no electron shell structure);[10] and 3) electron localization; an analysis of well-established bonding descriptors, such as the electron localization function (ELF),[11] can indicate electronic states consistent with a metallic picture of chemical bonding.[12]

Figure 1 shows a representative selection of the putative global minimum (GM) structures of zinc clusters, and photoelectron spectra of zinc cluster anions. The theoretical EDOS of anions simulate the photoemission spectra very well. We have additionally checked that the size dependence of the stabilities is in agreement with the well-known abundance mass spectra of both cations[17,18] and anions[18] (which we have reproduced in our experiment). The accuracy of the theoretical structures is therefore explicitly assessed. The spin multiplicity is the lowest possible one for all the GM structures, namely a singlet for neutral clusters and a doublet for singly-charged clusters.

Zinc clusters can be classified into two structural families. One (the adatom family; see $N = 11, 21, 48, 73$ as examples in Figure 1) features atoms with very low coordination in the GM, certainly an unexpected result for aggregates of a metallic element. Clusters of the other family do not have dangling atoms in the GM and behave in some aspects as typical metallic clusters. For example, their EDOS show a clear shell structure, with electron shell closings observed at

[*] Dr. A. Aguado, Prof. A. Vega
Department of Theoretical, Atomic and Optical Physics
University of Valladolid, Valladolid 47071 (Spain)
E-mail: aguado@metodos.fam.cie.uva.es
A. Lebon
Laboratoire de Magnètisme de Bretagne
29285 Brest Cedex (France)
Prof. B. von Issendorff
Physikalisches Institut, Universität Freiburg
H.-Herder-Strasse 3, 79104 Freiburg (Germany)

[**] We gratefully acknowledge the support of the Spanish "Ministerio de Ciencia e Innovación" and the European Regional Development Fund (Project No. FIS2011-22957). Facilities provided by the Pole de Calcul Intensif pour la Mer, CAPARMOR (Brest) are also acknowledged. The experimental work has been supported by the Deutsche Forschungsgemeinschaft.

Supporting information for this article is available on the WWW under http://dx.doi.org/10.1002/anie.201409835.

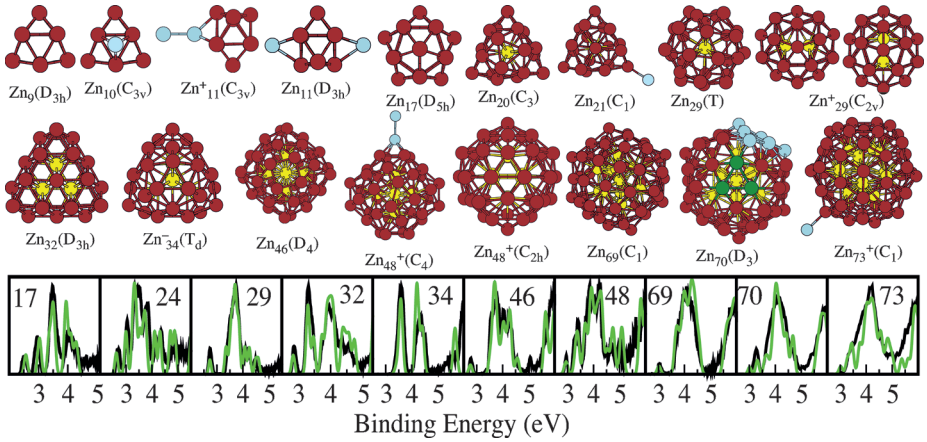

Figure 1. A selection of the putative GM structures and approximate point-group symmetries of zinc clusters. Internal (or core) atoms are shown in yellow, while blue is used to distinguish low-coordinate adatoms. For Zn_{70}, green and blue are used to highlight two different surface facets (see text). For Zn_{48}^+, we additionally show the first metastable isomer (C_{2h} structure). The bottom row compares the photoemission spectra for cluster anions (black lines) to the corresponding theoretical EDOS (green lines).

$N_e = 20$, 34, 40, 58, 70, 92, 138 electrons, which is compatible with a spherical superatom picture.[19] Moreover, their electron dipole moments are close to zero, and the s–p hybridization is already developed at $N = 9$. Thus, even if they show large HOMO–LUMO gaps at the shell closings (quantum confinement effects are unavoidable), many other features of the metallic state are already realized at size $N = 9$ within this family. But the presence of singly coordinated adatoms is not typical of metallic clusters, and they consistently appear at sizes following an electronic shell closing, coinciding with abrupt abundance drops in the mass spectra.[17,18] We will see below that the adatom family can be associated with reentrant insulating behavior.

The metallic structures themselves also display unusual properties. Starting from size 18 they can be described as endohedral clusters containing a core region surrounded by a crowded and rounded shell of atoms. Their two distinguishing features are a long radial distance separating the shell from the core and a large ratio of surface to core atoms. Typical interatomic distances within the core or the surface range between 2.6–2.7 Å and may be as short as 2.4 Å, while core–shell distances are 3.0 Å on average and may be as long as 3.3 Å. The long core–shell separation induces the lack of well-defined epitaxial rules for the growth of the shell onto the core, yet most structures are not amorphous and show a high point-group symmetry, opposing previous claims.[20,21] Some examples: Zn_{32} is a perfect hcp crystalline fragment; Zn_{34}^- has a high T_d symmetry; Zn_{29} has a single internal atom surrounded by a chiral shell with tetrahedral symmetry. An example of unclear epitaxy is provided by the C_{2h} isomer of Zn_{48}^+: its core is a 6-atom octahedron while the 42-atom shell is icosahedral. Another example is Zn_{70}, which features a 13-atom icosahedral core surrounded by a D_3 chiral shell: its growth pattern is Mackay-like on some facets (blue atoms in Figure 1), simple hexagonal and so much less compact on others (green atoms), and amorphous-like on the rest of facets, so different epitaxial rules may coexist within a single nanoparticle.

The partial decoupling between core and shell extends to the vibrational/dynamical properties. For some sizes, we locate competitive structures which differ just in the relative orientation of core and shell units. Zn_{29}^+, for example, has two degenerate GM structures (total energy difference lower than 1 meV), both featuring an internal dimer surrounded by a decahedral shell with D_{5h} symmetry. There are ten equivalent orientations of the dimer in each isomer, so a rotation of the dimer by $360/20 = 18$ degrees completes the interconversion between the two structures. The calculated transition barrier for this isomerization process is as low as 2.6 meV, that is, about 0.09 meV atom^{-1} (see the Supporting Information for an animation file containing the transition state geometry). Therefore, the dimer will be able to rotate inside the cage in a quasi-free manner. These results are supported by a calculation of the vibrational density of states or VDOS (vibrational frequencies and visualization of the normal modes are given in the Supporting Information). The softest mode has a very low frequency of 15 cm^{-1} and corresponds to the quasi-free rotation. Therefore, we predict that the dynamical decoupling might be detected in vibrational spectra in the form of very low frequency tails. An additional exotic feature of the VDOS is that the stiffest mode does not involve the core atoms and is rather localized in the shell region. This behavior, induced by the crowded atomic population of the shell, is the opposite to the one seen in other typical metals.[22]

The physical reasons for these exotic properties can be elucidated by an analysis of the electronic properties. We start by discussing the adatom family. The electronic structure of two $N/N+1$ cluster pairs, with $N = 10$ or 20, is analyzed in Figure 2. In both cases, the $(N+1)$-cluster is obtained by adding a low-coordinate adatom to the N-atom cluster, which itself is a magic superatom with a closed electronic shell. For Zn_{11} we show results for two competitive structures that differ just in the spatial location of the adatom. Both Zn_{10} and Zn_{20} display a jellium-like sequence ($1S^2 1P^6 1D^{10} 2S^2 1F^{14} 2P^6 \ldots$) of delocalized electronic levels, apart from a small crystal-field splitting due to a non-perfectly spherical shape. As an example, we show the electron density of the 2S orbital of the C_{3v} isomer (this plot is similar for both Zn_{10} and Zn_{11}), which clearly resembles an atomic 2s-orbital. Even for Zn_{10}, the HOMO contains roughly an equal proportion of s- and p-orbitals, while for Zn_{20} the HOMO is already dominated by p-orbitals; the LUMO is predominantly p-like in all cases. This hybridization could be interpreted as an overlap of the s-band and the p-band; so if one does not consider the vanishing of

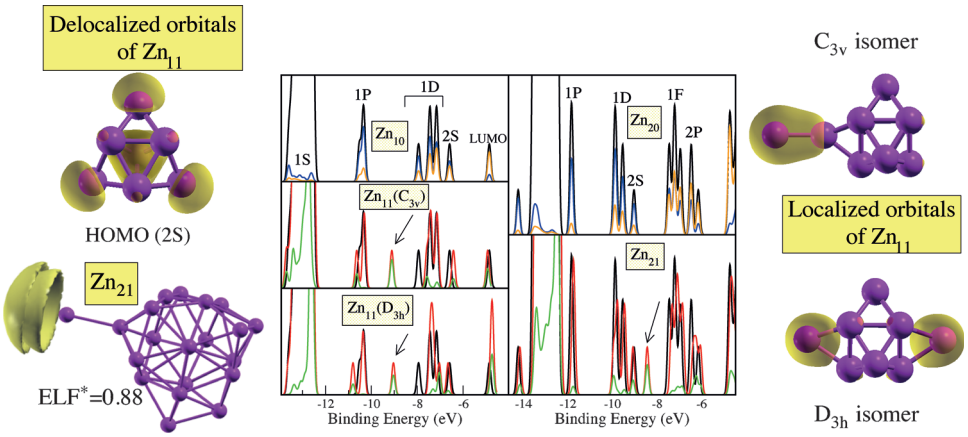

Figure 2. Center: comparison of the EDOS of two $N/N+1$ cluster pairs. Black lines give the EDOS of Zn_{10} and Zn_{20}; red lines give the EDOS of Zn_{11} and Zn_{21}; blue and orange lines show the contribution of s- and p-orbitals to the EDOS, respectively; green lines show the contribution of the adatom plus the atom(s) to which it is bonded. The new peak that appears at size $N+1$ is marked with an arrow. Bottom left: an ELF isosurface at 88% of its maximum value for Zn_{21}. The other three plots show the local contribution of the insulating peak (right side) and of the HOMO (left side) to the electron density of Zn_{11}.

the bandgap, but instead the occurrence of this overlap as a criterion for metallicity, zinc clusters are already metallic at the smallest sizes considered in this paper. This is in agreement with previous theoretical results on small Zn clusters[23].

In metallic systems, it would be expected that the additional electrons in the $(N+1)$-cluster populate the LUMO of the N-cluster; that is, the state above the bandgap. What is surprising is that the additional atom rather takes an insulating option, because its filled orbitals contribute a newly formed state below the bandgap without significantly disturbing the EDOS of the metallic host. This is more like what occurs when an atom is added to a separate band insulator. In such a case the filled orbitals of the atom would add to the fully occupied valence band level manifold, while its empty orbitals would become part of the unoccupied conduction band levels. An independent confirmation of insulating behavior comes from an analysis of the electron density distribution. The ELF of Zn_{21} has a maximum value $ELF_M = 0.85$, suggesting strong localization. An isosurface plot at $ELF^* = ELF/ELF_M = 88\%$ (bottom left corner) shows that the region of strongest localization occurs just on top of the adatom, implying a lone electron density contribution. This adatom attractor merges with the attractors in the metallic part (see below) only at a very low bifurcation value of $ELF^* = 25\%$, which suggests that the $Zn{-}Zn_{20}$ bond (or adatom–superatom bond) is not a metallic bond. The total electron density also shows a deep minimum (that is, a charge depletion) in the bond region, hinting at a rather non-bonding interaction. Nevertheless, the dissociation energy of Zn_{11}^+, for example, is about 0.8 eV, so the interaction is certainly stronger than expected for a van der Waals bond. A Bader analysis reveals a charge transfer from the adatom to the metallic part of about 0.2 electrons, showing that the adatom–superatom bond has a partially ionic nature.

The insulating character is revealed also in the spatial localization of the electron density contributed by the newly formed orbital. The electron density of the insulating level of Zn_{11} (C_{3v}) is visualized on the upper right corner through an isosurface at 15% of its maximum value, and it is clearly localized at the adatom region. The D_{3h} isomer is interesting because the adatom site is equivalent by symmetry to one of the atoms of Zn_{10}. The electron density of the new level below the bandgap is shown on the bottom right corner. It demonstrates also electron localization, but now shared between the two atoms which are equivalent by symmetry. Herein we find an interesting quantum resonance phenomenon, with the ground state being a coherent quantum superposition of the two equivalent possibilities to place the insulating bond. The green curves in the EDOS plot show the partial contribution of the adatom plus the atom(s) to which it is bonded to the total EDOS. It recovers more than 80% of the newly added peak, further confirming the localization properties. For the neutral clusters shown in Figure 2, the energy of the new peak in the EDOS is very close to the ionization potential of an isolated Zn atom (9.3 eV), while the rest of electron energy levels continue to be of a delocalized jellium nature. The whole analysis provides evidence that two different electronic phases, namely metallic and insulating, coexist within a single nanoparticle, which can thus be classified as Janus-like. This very exotic coexistence has, not surprisingly, unusual consequences. For example, the HOMO–LUMO gap of Zn_{11} (D_{3h}) is even larger than that of Zn_{10}, because no new electronic shell is yet opened.

We next analyze the metallic family in Figure 3. We show plots of the density difference $\Delta\rho = \rho - \rho_{atm}$, with ρ_{atm} the promolecular density. Positive (negative) values of $\Delta\rho$ correspond to electron density accumulation (depletion), respectively. In Zn_{29}, whose polyhedral shell contains only triangular facets, the $\Delta\rho = +0.006$ isosurface is the dual (or reciprocal) of the shell polyhedron; that is, its vertices coincide with the centers of the triangular faces of the shell. This isosurface displays a connected network of three-center bonds. There are no features connecting the innermost atom to the shell at this $\Delta\rho$ value, implying that the radial bonding between core and shell is much weaker than the tangential bonding within the shell. The electron density accumulated at the shell has to be extracted from other cluster regions, which are visualized in the $\Delta\rho = -0.002$ isosurface. Part of the charge comes from the outer region of the shell atoms, which becomes more delocalized as expected in a metal. But the relatively hollow region separating core and shell is also a region with significant electron deficit.

These features are best appreciated in the isoline plot, which shows deep purple regions only across the shell and

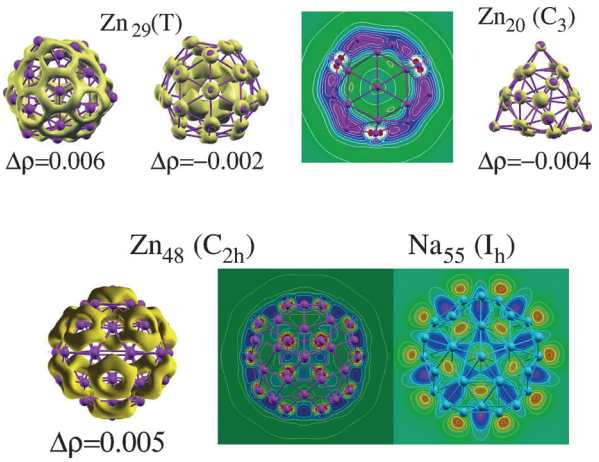

Figure 3. Isosurfaces of constant $\Delta\rho$ (in a.u.). Also shown are some contour slices through appropriate planes, both for selected zinc clusters and Na_{55}. A rainbow color scale is employed in the isoline plots, with a linear interpolation between the minimum (red) and maximum (purple) values of the function.

a wide green region separating core and shell. A light blue ring about the central atom (corresponding to $\Delta\rho = +0.001$) is the only trace of a very weak, angularly delocalized, radial bonding. The $\Delta\rho = -0.004$ isosurface of Zn_{20} illustrates the different electronic behavior of core and shell atoms. The electron density of the internal atom delocalizes in an spherically symmetric way, trying to enhance the cohesion to the shell as a whole. Meanwhile, the shell atoms lose their charge along the tangential directions, enhancing only the cohesion within the shell. Interactions in zinc clusters are thus isotropic within the core but directional within the shell, resembling a nanoalloy with two different metallic species rather than a one-component system. A population analysis of the cluster wavefunction reveals that, while in the core atoms the p-population is equally shared between p_x, p_y, and p_z orbitals, the population of the radial p-orbital is essentially zero for the shell atoms. The connected network of three-center bonds identified at the shell is therefore achieved through something similar to a sp^2-hybridization (which, due to the different number of valence electrons and character of the bonds, is of course different in its details to the standard sp^2-hybridization in, for example, carbon).

These observations hold for all other sizes, including those with more than one core atom. The peculiar behavior of zinc clusters is best illustrated through a comparison with a more typical metallic cluster. In Figure 3, we compare the C_{2h} isomer of Zn_{48}^{+} to Na_{55}. These clusters share a common icosahedral shell with 42 atoms, which encapsulates either a 6-atom octahedron (Zn_{48}^{+}) or a 13-atom icosahedron (Na_{55}). The contour slices clearly reveal a strong radial bonding gluing the core and shell of Na_{55}, a feature which is absent in Zn_{48}^{+}. Moreover, we did not observe any indication of sp^2-hybridization in Na_{55}, where all the atoms contribute some charge in an isotropic way to ensure metallic cohesion.

An analysis of the ELF for clusters of the metallic family (Supporting Information, Figure S1) confirms all the conclusions obtained from the $\Delta\rho$ analysis. The maximum value of the ELF is below 0.5, which is indicative of a delocalized density distribution with metallic cohesion. Also, while the several ELF attractors located at the shell already merge together at ELF* = 90%, the core and shell attractor basins fully connect with each other only at a very low bifurcation value of ELF* = 25%. This amounts to an absolute value of ELF = 0.11, which is of the same order of magnitude as the ELF minima observed in between ions of typical insulating crystals.[24] Therefore, core and shell regions of zinc clusters are as weakly connected as two units of an insulating system. The same conclusion can be reached from total density values: as compared to the average free electron density of 0.019 a.u. in bulk zinc, the total electron density is as low as 0.002 a.u. at its minimum between the core and shell regions of Zn_{29}, that is, roughly an order of magnitude decrease. The physical picture that emerges from this analysis is that of two largely independent metallic phases, a 2D metal at the shell and a 3D metal at the cluster core, which only weakly interact with each other but coexist within the same nanoparticle. This explains the lack of clear epitaxial rules for growth of the shell onto the core and the partial dynamical decoupling between core and shell. It is also tempting to think that the very stable and distant shell can isolate the core from external influences to a high degree, thus providing a natural protective coating for the internal zinc metal and maybe also for other encapsulated metals. Although this idea still has to be explicitly checked, we believe it may be a key factor in explaining the widespread use of zinc in corrosion protecting layers.

The present work approaches the problem of metallicity in nanostructures by analyzing in detail the chemical bonding pattern and electronic density distribution in real space, as well as the EDOS in energy space. While in two former publications[1,4] based on experimentally determined HOMO–LUMO gaps a transition from an insulator to a simple free-electron metal in zinc clusters was suggested to occur at size 32, the theoretical analysis reveals a much more complex situation. On one hand, a cluster as small as Zn_9 already displays many features of a metallic-like cohesion, despite having a sizable HOMO–LUMO gap. On the other hand, the larger clusters up to size 73 exhibit some properties which are far from simple-metal-like behavior. The insulator–metal transition is thus not at all a sharp transition occurring at a well-defined size, but rather a smooth change of properties, which most probably will continue even for much larger cluster sizes.

Our work is a significant step towards a deeper understanding of the metal–insulator transition in nanoparticles, and provides fundamental physical insights on the meaning of the concept of metallicity. In particular, we have provided the first evidence for the exotic coexistence of two different electronic phases (metallic and insulating) within a single Janus-like nanoparticle. Additionally, we have demonstrated that the metallic clusters contain two largely independent metallic phases with different dimensionality, namely an sp^2-bonded 2D-metal at the shell and an isotropic 3D-metal at the core. The unique properties of zinc clusters identified herein open fascinating new avenues also for applied research. In particular, Zn shells may serve as nanocoatings that effec-

tively isolate the cluster interior from external influences and thus may help to preserve its potentially interesting properties. Work along these lines is presently in progress.

Methods

Photoelectron spectra of zinc cluster anions were measured employing the same methods as described earlier.[1,4] Briefly, zinc clusters were produced in a magnetron sputter gas aggregation source, thermalized to about 100 K in a liquid-nitrogen-cooled radio-frequency ion trap, mass-selected in a time-of-flight mass spectrometer, and irradiated by an ArF excimer laser ($h\nu = 6.4$ eV) in the interaction region of a magnetic bottle type time-of-flight photoelectron spectrometer. The arrival-time spectra of the emitted electrons have then been transformed to the binding energy spectra shown in Figure 1. Putative GM structures were initially determined through unbiased basin hopping[13] optimizations based on a Gupta potential,[14] and later on reoptimized (for both neutral and singly charged clusters) at the DFT level employing the SIESTA code[15] and the PBE exchange-correlation functional.[16] Full computational details and benchmark accuracy tests are given in the Supporting Information.

Received: October 7, 2014
Revised: November 12, 2014
Published online: December 22, 2014

Keywords: corrosion-protecting coatings · insulating states · metallic states · zinc clusters

[1] B. von Issendorff, O. Cheshnovsky, *Annu. Rev. Phys. Chem.* **2005**, *56*, 549 – 580.
[2] R. Kubo, *J. Phys. Soc. Jpn.* **1962**, *17*, 975 – 986.
[3] R. Busani, M. Folkers, O. Cheshnovsky, *Phys. Rev. Lett.* **1998**, *81*, 3836 – 3839.
[4] O. Kostko, G. Wrigge, O. Cheshnovsky, B. von Issendorff, *J. Chem. Phys.* **2005**, *123*, 221102.
[5] O. Thomas, W. Zheng, S. Xu, K. Bowen, *Phys. Rev. Lett.* **2002**, *89*, 213403.
[6] J. Bowlan, A. Liang, W. A. de Heer, *Phys. Rev. Lett.* **2011**, *106*, 043401.
[7] A. Aguado, A. Vega, L. C. Balbás, *Phys. Rev. B* **2011**, *84*, 165450.
[8] A. Aguado, A. Largo, A. Vega, L. C. Balbás, *Chem. Phys.* **2012**, *399*, 252 – 257.
[9] L. Ma, K. A. Jackson, J. Wang, M. Horol, J. Jellinek, *Phys. Rev. B* **2014**, *89*, 035429.
[10] G. Wrigge, M. A. Hoffmann, B. von Issendorff, H. Haberland, *Eur. Phys. J. D* **2003**, *24*, 23 – 26.
[11] A. D. Becke, K. E. Edgecombe, *J. Chem. Phys.* **1990**, *92*, 5397 – 5403.
[12] R. Rousseau, D. Marx, *Chem. Eur. J.* **2000**, *6*, 2982 – 2993.
[13] D. J. Wales, J. P. K. Doye, *J. Phys. Chem. A* **1997**, *101*, 5111 – 5116.
[14] F. Cleri, V. Rosato, *Phys. Rev. B* **1993**, *48*, 22 – 33.
[15] J. M. Soler, E. Artacho, J. D. Gale, A. García, J. Junquera, P. Ordejón, D. Sánchez-Portal, *J. Phys. Condens. Matter* **2002**, *14*, 2745 – 2780.
[16] J. P. Perdew, K. Burke, M. Ernzerhof, *Phys. Rev. Lett.* **1996**, *77*, 3865 – 3868.
[17] T. Diederich, T. Döppner, Th. Fennel, J. Tiggesbäumker, K.-H. Meiwes-Broer, *Phys. Rev. A* **2005**, *72*, 023203.
[18] O. Kostko, Ph.D. the*sis*, University of Freiburg, **2007**.
[19] a) M. Brack, *Rev. Mod. Phys.* **1993**, *65*, 677 – 732; b) P. Jena, *J. Phys. Chem. Lett.* **2013**, *4*, 1432 – 1442.
[20] K. Michaelian, M. R. Beltrán, I. L. Garzón, *Phys. Rev. B* **2002**, *65*, 041403.
[21] J. P. K. Doye, *Phys. Rev. B* **2003**, *68*, 195418.
[22] H. E. Sauceda, F. Salazar, L. A. Pérez, I. L. Garzón, *J. Phys. Chem. C* **2013**, *117*, 25160 – 25168.
[23] J. Wang, G. Wang, J. Zhao, *Phys. Rev. A* **2003**, *68*, 013201.
[24] J. Contreras-García, J. M. Recio, *J. Phys. Chem. C* **2011**, *115*, 257 – 263; J. Contreras-García, A. M. Pendás, J. M. Recio, *J. Phys. Chem. B* **2008**, *112*, 9787 – 9794.

